ELSEVIER

Infrared Physics & Technology 41 (2000) 271–281

INFRARED PHYSICS & TECHNOLOGY

www.elsevier.com/locate/infrared

Measurement of the resonant lengths of infrared dipole antennas

Christophe Fumeaux, Michael A. Gritz, Iulian Codreanu, William L. Schaich [1], Francisco J. González, Glenn D. Boreman *

School of Optics/CREOL, University of Central Florida, P.O. Box 126700, Orlando, FL 32816-2700, USA

Received 27 April 2000

Abstract

The resonant lengths of infrared dipole antennas at 10.6 and 3.39 μm are experimentally investigated. For this purpose, submicron-sized microbolometers coupled to dipole antennas with lengths between 0.7 and 20 μm were fabricated on a SiO_2-on-Si substrate. The response of the detector to 10.6 μm radiation shows a first resonance for an antenna length between 1.0 and 2.5 μm. A subsequent zero and a second attenuated resonance are observed as the antenna length increases. Similar behavior is observed for illumination at 3.39 μm, with a first resonance occurring at a length shorter than 1 μm. The results permit evaluation of an effective dielectric permittivity and shows the effect of the surface impedance of the metal on the propagation of current-wave on the antenna. The resonance behavior is further studied by changing the irradiation conditions of the detectors. Air-side and substrate-side illumination exhibit identical resonant antenna lengths, but different efficiencies of power collection. The antenna patterns as a function of incident angle have also been measured at 10.6 μm, showing a transition from a primary broadside lobe to the development of side lobes for longer antennas. Finally, an antenna response is measured at visible frequencies. Our measurements point out similarities, as well as differences, between infrared antennas and their counterparts at microwave frequencies, and provide insights useful for the design optimization of planar infrared antennas.

Keywords: Infrared antenna; Microbolometer; Infrared detector

1. Introduction

Infrared antennas are used to collect incident power and apply it as an alternating signal at THz frequencies to a detector with dimensions much smaller than the wavelength. The separation of the power collection and sensing functions of the detector permits optimization of both functions independently. This concept leads to numerous possible combinations of shapes and materials for both the sensor and its antenna. The types of submicron-sized sensors include thermal devices like microbolometers [1,2] or thermocouples [3], and nonlinear junctions such as metal–oxide–metal (MOM) diodes [4,5], Josephson junctions [6,7] and Schottky diodes [8]. The small size of the

* Corresponding author: Tel.: +1-407-823-6815; fax: +1-407-823-6880.

E-mail address: boreman@creol.ucf.edu (G.D. Boreman).

[1] Permanent address: Department of Physics, Indiana University, Bloomington, IN 47405, USA.

1350-4495/00/$ - see front matter
PII: S1350-4495(00)00047-5

detector is essential to obtain a fast response and low-noise room-temperature operation [9]. In the case of the nonlinear junctions, the small size also permits maintenance of the nonlinear I–V characteristics up to extremely high frequencies for applications as THz mixers. Many planar-antenna designs are feasible and can be tailored according to the application: dipole [4], bow-tie [3,5], spiral [1,5], log-periodic [3], slot-antenna [10], and microstrip patches [2]. Infrared antenna-coupled detectors also find applications in thermal imaging, as ultrafast polarization-sensitive detectors [11] and as low-noise heterodyne detectors. The design of infrared antennas requires to take into account effects that can be neglected at microwave frequencies. Resonance features are altered because the propagation of THz-frequency antenna current-waves is affected by the large high-frequency complex surface impedance of the metal. In this study, we use Nb microbolometers coupled to dipole antennas of several lengths to investigate the resonances of infrared dipole antennas on a SiO_2-on-Si substrate.

The study of the response of the detectors with different antenna lengths at fixed wavelengths in the atmospheric windows (8–12 and 3–5 μm) permits determination of the resonances of planar metallic structure in the infrared. The results help us to determine the role of the underlying substrate and the high-frequency propagation of the antenna currents on the metallic dipole arms. These observations yield guidelines for the fabrication of future infrared antennas.

2. Structures and fabrication

Fig. 1 shows an electron microscope photograph of the type of devices used in this study. The entire structure is defined with electron-beam lithography. The arms of the dipole antenna and the dc leads are both made of Au in one lithographic step. We fabricated antennas with 30 different lengths between 0.7 and 20 μm. The width of the antenna is approximately 200 nm for all the devices and the gap between the two arms is 400 nm. The thickness of the Au layer is 100 nm.

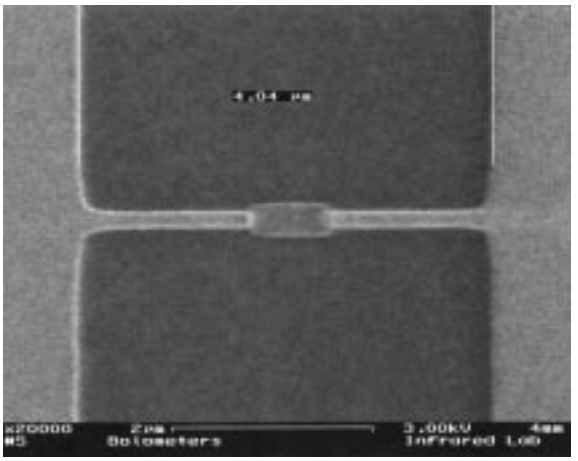

Fig. 1. Electron micrograph of an antenna-coupled Nb bolometer.

The sensor at the feed of the antenna is a sputtered 0.8 μm × 0.3 μm Nb patch with a thickness of 70 nm. The choice of a Nb patch as the bolometric sensor permits us to obtain highly homogenous and reproducible devices because of the relative ease of fabrication compared to nonlinear contacts. The bulk dc conductivity of Nb is six to seven times lower than that of Au. Not surprisingly, our thin-film Nb patches have even lower conductivity and form a load resistance that is approximately impedance-matched to the antennas. The average dc resistance of the devices is around 140 Ω.

The substrate is a 380-μm-thick high-resistivity Si wafer ($\rho \approx 3$ kΩ cm). Both sides were polished, and then coated with 200 nm of thermally grown SiO_2 for thermal and electrical isolation. The spectral properties of the substrate were measured with a Fourier-transform infrared (FTIR) spectrometer and yielded a power transmission through both surfaces of 67% at 3.39 μm and 52% at 10.6 μm.

3. Experimental method

The measurement of the resonance of antennas is usually performed by varying the frequency of the incident radiation. At infrared frequencies, this

approach would require a source tunable over a wide range and a frequency-independent optical train. In addition, the materials used in the fabrication of the devices would need to have truly wavelength-independent properties over a wide range in order not to alter the results. To overcome these difficulties, we used an alternate approach. We compared the responses of microbolometers coupled to antennas of several different lengths to infrared radiation at specific wavelengths. To minimize effects such as variation of bolometer resistance caused by the fabrication process, all the devices tested were located on the same wafer and consequently fabricated under strictly identical conditions. The chips were mounted on chip carriers permitting illumination in two configurations: one directly from the air side, and another through the substrate.

The main study was carried out using CO_2-laser emission at 10.59 μm (10P (18)). The laser beam was focused by an $F/1$ optical train, resulting in an almost diffraction-limited spot with a $1/e^2$ radius of 12 μm and an irradiance of approximately 1000 W/cm^2 at focus. The polarization was linear and was rotated by means of a half-wave plate. The bolometer under test was biased at 100 mV and placed at the focus of the laser beam. The position of the device was adjusted for best response using motorized stages with submicron accuracy. The laser beam was modulated with a chopper at a frequency of 2.5 kHz and the modulated signal produced by the bolometer was read with a lock-in amplifier after a 10× preamplification. For each device, we measured at normal incidence the response $V_{\parallel}$ to radiation polarized along the dipole arm, and the response $V_{\perp}$ for the cross-polarization. The residual variation of resistance among bolometers was removed from the measured signals by normalization to a device resistance of 140 Ω, taking into account the proportionality of the signal voltage to the resistance of the bolometer.

The use of the tightly focused $F/1$ radiation was advantageous for the illumination-through-the-substrate configuration. Because of the large divergence of the beam, power reflected at the back-side of the 380-μm-thick Si substrate produced only negligible irradiance contributions on the detector. This avoided interference effects caused by multiple reflections in the Si substrate, which have been observed in larger $F/\#$ systems [5]. However, for the antenna pattern measurements as a function of the angle of incidence from the air side, the optics was changed to an $F/2$ system to reduce the effect of the convolution of the antenna pattern with the angular distribution of the focused light cone. In the case of air-side illumination, the large bond pads situated on both sides of the antenna reflected most of the radiation before entering the substrate, so that interferences were not observed, even with the higher $F/\#$.

The optical train was built according to the same principles for the other wavelengths used in this study. An IR HeNe laser was operated at 3.39 μm, and a visible HeNe laser at 632.8 nm. The main difference was in the focusing conditions. At 3.39 μm, the spot at the focus of the $F/1$ system was not diffraction-limited due to a poorer beam quality of the laser. In the visible, an $F/4$ setup was chosen to obtain a focal spot with a radius of about 3 μm, so that the measured antennas with $L \leqslant 6$ μm were completely illuminated when placed in the focus of the beam.

Table 1
Illumination conditions and measured signals at the three wavelengths used in the study[a]

Wavelength λ_0	Beam power (mW)	Focusing optics	Radius at focus (μm)	Approximate irradiance (W/cm^2)	Maximum signal ΔV (μV)	Irradiance responsivity at maximum (μV/(W/cm^2))	Polarization ratio V_{max}/V_{min}
10.59 μm	5	$F/1$	12	1000	413	0.41	15
3.39 μm	<0.5	$F/1$	~8	<220	28	0.13	5
632.8 nm	~2.5	$F/4$	3	7900	450	0.06	3

[a] The irradiance responsivity and polarization ratios are given for the maximum signals measured. The results in the infrared (first two rows) are for substrate-side illumination, whereas the results in the visible (last row) are for air-side illumination.

The irradiance conditions at the different wavelengths are summarized in the first columns of Table 1.

4. Experimental results

4.1. Length study at 10.6 μm

We measured the response of antenna-coupled bolometers to 10.6 μm radiation incident from the substrate side for 30 lengths L (full length) of the dipole between 0.7 and 20 μm. For all the antenna lengths tested, the maximum signal V_{max} was obtained for the polarization parallel to the antenna axis and the minimum signal V_{min} for the cross-polarization, i.e. $V_{||} = V_{max}$ and $V_{\perp} = V_{min}$. Ratios V_{max}/V_{min} between the co- and cross-polarized signals up to 15 were observed. The polarization-dependent signal $\Delta V = V_{max} - V_{min}$ as a function of full length L is plotted in Fig. 2. Each point corresponds to the average of four devices with the same antenna length, the error bars indicating the measured standard deviation for each data point. The signal V_{min} for perpendicular polarization is mainly of thermal origin and is not shown because it is small and independent of the antenna length.

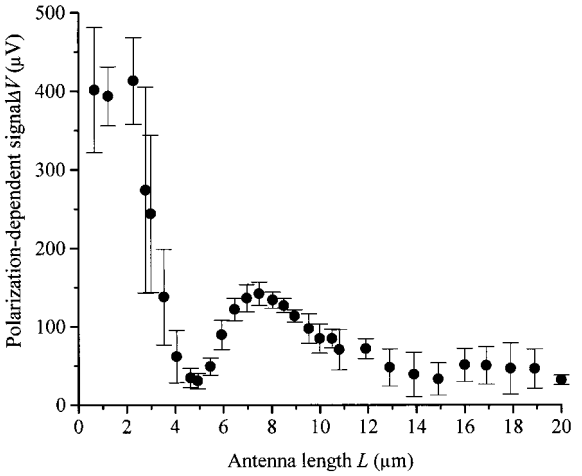

Fig. 2. Polarization-dependent response ΔV of the bolometers as a function of the antenna length L at 10.6 μm (average and standard deviation for four devices at each point).

The measured curve exhibits a first resonance for short antennas with a length L shorter than 2.5 μm. This first resonance is not well defined in our measurement for several reasons. A precise determination of the resonance at these short lengths would require smaller increments in the fabricated lengths L and smaller standard deviation in the measurements. In addition, the size of the bolometer patch compared to the length of the antenna and the presence of the large bond pads likely modifies the behavior of the antennas for the shortest lengths fabricated. Past the first resonance, the curve of Fig. 2 exhibits a first minimum for $L \approx 5$ μm and a second maximum for $L \approx 7.5$ μm. The magnitude of the second maximum is about one third that of the first resonance, and is broadened on the long-L side. For lengths longer than this second resonance, the curve exhibits a slow decay, with no clearly distinguishable oscillating structure within the standard deviation of our measurements.

The resonances of the curve are certainly broadened by the use of focused light, since the illumination occurs not only at normal incidence, but over a distribution of angles determined by the $F/1$ focusing optics.

4.2. Interpretation of the results at 10.6 μm

The interpretation of the resonant lengths in terms of the free-space wavelength of the incident radiation is not straightforward because of the presence of the layered substrate. Since the location and structure of the first antenna resonance have not been determined with precision, our interpretation will be based on the observation made on the curve of Fig. 2 past the first resonance.

We first consider the mechanism by which an antenna signal is produced in our devices. The predominant process leading to the rise in temperature of the microbolometer is the dissipation of antenna currents in the Nb. The heat produced generates a signal by changing the resistance of the device. This signal is dependent on the power collected and consequently on the polarization used and on the collection efficiency of the antenna. Other mechanisms, such as the absorption

of optical power in the substrate, generate signals nearly independent of polarization. These other mechanisms are not considered here since they do not contribute to the polarization-dependent part of the signal ΔV.

The way our device operates corresponds to sensing the power of the alternate current dissipated in the middle portion of an excited gold wire. The bolometer, which is essentially a piece of metal with a higher resistivity located in the middle of the Au antenna, is considered only a small perturbation with no significant effect. Hence, we consider our antennas as thin receiving antennas excited by a plane wave with the electric field parallel to the antenna. The distribution of current and charge along such a conductor in free space is given in [12]. The shortest length that exhibits zero current in the center of the ideal receiving antenna corresponds to a full length L of 2λ of the incident radiation. In our measurement at a wavelength of 10.6 μm (Fig. 2), the first minimum of the response for $L \approx 5.0$ μm represents one of the most distinguishing characteristics of the curve. We interpret this first minimum as corresponding to the 2λ null of the current distribution at the center point of the ideal antenna. The measured width of the first resonance is broad enough to contain the resonances of structures with current distributions exhibiting $\lambda/2$, λ and $3\lambda/2$ characteristics.

For transmission lines, the propagation of currents on a planar metallic structure on top of a substrate is described with the help of an "effective permittivity" ε_{eff}. The propagation is then approximated as if the metallic structure were fully immersed in a medium with permittivity ε_{eff}, (or index of refraction n_{eff}) that defines an effective wavelength $\lambda_{\text{eff}} = \lambda_0/(\varepsilon_{\text{eff}})^{1/2} = \lambda_0/n_{\text{eff}}$. This effective permittivity ε_{eff} is dependent on the dielectric permittivity of the different materials involved, on the geometry of the structure, and on the frequency of the propagating currents. At low frequencies, in the quasi-static domain, ε_{eff} is close to the average between the permittivity of the substrate and the permittivity of vacuum. As the frequency increases, the effective permittivity also increases. The high-frequency asymptotic value of ε_{eff} is given by the permittivity of the substrate [13]. The transition from one domain to the other is relatively steep and the inflection point depends on the geometry and size of the structure relative to the free-space wavelength of interest. Since the wavelength is comparable to the size of our antennas, we expect an effective index with a magnitude between the quasi-static value and the high-frequency limit.

For our infrared antennas, the interpretation of the first zero as the 2λ resonance defines an apparent wavelength $\lambda_{\text{app}} \approx 2.5$ μm for incident 10.6 μm radiation. This value of λ_{app} is 20% shorter than the high-frequency asymptotic limit $\lambda_{\text{eff,min}} \approx \lambda_{\text{Si}} \approx 3.1$ μm. This result can be qualitatively explained by considering the role of the complex surface impedance of the metal $Z_{\text{S}} = R_{\text{S}} + \text{i}X_{\text{S}}$ at high frequencies as described in [14]. The surface resistance R_{S} causes an attenuation of current waves on the metal, and the surface inductance X_{S} induces a change in the propagation constant. This change is equivalent to a shortening of the wavelength of the propagating current wave. The effect of the surface reactance is negligible at low frequencies, but becomes more important as the frequency increases. At infrared frequencies, the surface reactance of Au has a higher magnitude than its surface resistance.

In the following, we estimate the shortening of the effective wavelength caused by surface reactance on our antennas illuminated with 28.3 THz radiation (10.6 μm free-space wavelength). Starting from the optical properties of Au tabulated in [15] for infrared frequencies, we determine the complex conductivity of the metal at 28.3 THz with the help of the linking equations given in [16]. The complex surface impedance Z_{S} can then be estimated [17] as follows:

$$Z_{\text{S}} = R_{\text{S}} + \text{i}X_{\text{S}} = (\text{i}\omega\mu_0/\sigma)^{1/2}, \tag{1}$$

where ω is the angular frequency, μ_0 is the magnetic permeability of vacuum and σ is the complex conductivity of the metal at 28.3 THz, with real part $\sigma_{\text{R}} = 2.6 \times 10^6\ \Omega^{-1}\,\text{m}^{-1}$ and imaginary part $\sigma_{\text{I}} = 7.3 \times 10^6\ \Omega^{-1}\,\text{m}^{-1}$. This yields for Au a value of $R_{\text{S}} = 0.92\ \Omega$ and $X_{\text{S}} = 5.28\ \Omega$ at 28.3 THz. Approximating the antenna as a transmission line, a first-order approximation of the change in propagation constant $\Delta\beta$ is given by [14]

$$\Delta\beta \approx \alpha \frac{X_S}{R_S}, \tag{2}$$

where α is the attenuation constant of current waves on the metal expressed in inverse length units.

The approximate determination of the current-wave attenuation constant α is based on our observation of the curve of Fig. 2. The flat curve for large antenna length (Fig. 2 for $L > 10$ μm) indicates that the longest measured antennas resemble an infinitely long antenna. We can consequently estimate the attenuation α by estimating the distance L_r over which the power of a current wave has fallen to $1/e^2$ of its original value according to

$$e^{-2\alpha L_r} = 1/e^2 \quad \text{or} \quad \alpha L_r = 1. \tag{3}$$

This distance L_r also corresponds to the length where the oscillations in the resonance curve disappear. We consequently estimate $\alpha \approx 0.1$ μm^{-1} for $L_r \approx 10$ μm.

The ratio X_S/R_S calculated from Eq. (1) is around 5.7 at a frequency of 28.3 THz, so that the change of propagation constant $\Delta\beta$ and consequent shortening of the effective wavelength can be estimated according to Eq. (2). We can further write

$$\beta_{measured} = 2\pi/\lambda_{app} = \beta_{eff} + \Delta\beta = 2\pi/\lambda_{eff} + \Delta\beta. \tag{4}$$

Introducing the measured value of the effective wavelength $\lambda_{app} \approx 2.5$ μm, we estimate an effective wavelength equal to $\lambda_{eff} \approx 3.25$ μm. This value is slightly longer than the wavelength λ_{Si} of the incident radiation in the Si substrate. The effective wavelength of the current waves is consequently a wavelength located between the quasi-static value and the asymptotic high-frequency value. The apparent wavelength is shorter than the effective wavelength because of surface-impedance effects [14]. A more precise computer simulation of the structure is in progress and is expected to characterize the effective index with more accuracy.

The relatively high attenuation of antenna currents on our structures is the primary cause of the broadening and smoothing of the resonances observed. In addition, illumination over an angular range around normal incidence resulting from the $F/1$ optics also contributes to this behavior.

4.3. Substrate-side versus air-side illumination

An antenna at an interface of two dielectrics radiates most of its energy on the side with the higher permittivity [18]. Reciprocally, an antenna on a substrate will collect radiation incident from the substrate side more efficiently than radiation incident from the air side.

We compared directly the response of the antenna-coupled detectors to the two types of illumination. A group of bolometers with antenna lengths L from 0.7 to 11 μm were first illuminated through the substrate and then from the air side. Illumination was at normal incidence and a wavelength of 10.6 μm. The antenna responses ΔV of the devices are plotted for both illumination types in Fig. 3 as a function of the antenna length. Comparison of the two curves yields the following observations. First, the locations of the resonances are identical for both illuminations although the dielectric wavelengths of both incident beams (in air and Si/SiO_2) are different. This confirms that the resonances are effectively determined by the propagation of antenna currents described with the help of an effective dielectric constant for the metallic structure on the substrate. Secondly, the

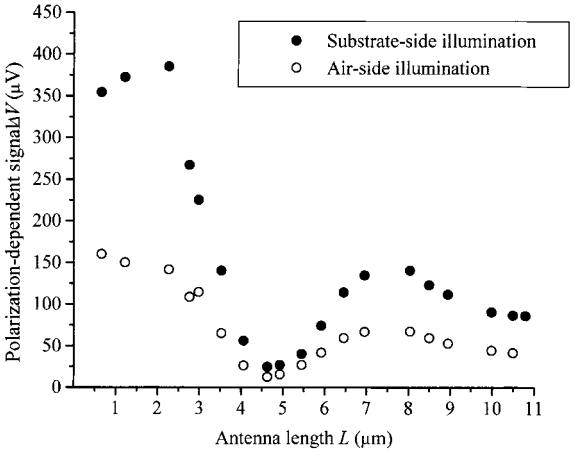

Fig. 3. Direct comparison of bolometer antenna response at 10.6 μm wavelength for air-side and substrate-side illumination as a function of the antenna length L.

signals are higher for substrate side illumination by a factor 2.1 ± 0.3 for the full range of antenna lengths. Considering that only 52% of the power is transmitted through our substrate at 10.6 μm, we estimate that coupling of power to the antenna from the substrate side is at least four times more efficient than from the air side.

It is likely that the efficiency of coupling from the substrate side is even more than four times the efficiency of coupling from the air side. In our present configuration, the signal measured for air-side illumination is enhanced by coupling of power to the antenna that occurs also from the substrate side after reflection at the first SiO_2/Si interface in the substrate [19].

4.4. Antenna patterns

The response of microbolometers as a function of the angle of incidence was measured for four different antenna lengths: 1.2, 2.5, 4.6 and 7.5 μm. The first two lengths are within the first resonance, whereas the third and fourth lengths are close to the first zero and the second resonance, respectively. The antenna pattern measurements were performed for angles between normal incidence and 72° in the *E*-plane, defined as the plane perpendicular to the substrate that contains the dipole antenna. The devices were illuminated from the air side. After each increment of the incidence angle, the device was realigned and the signal was measured for both s- and p-polarizations. The optics used for these measurements was $F/2$, to reduce the effect of convolution with an angular window that would result from the use of a lower $F/\#$. The upper angle limit was set by space limitations between the focusing lens and the chip holder.

The dependence of the antenna signals ΔV on the angle of incidence for the lengths given above are shown in Fig. 4. All the patterns are normalized to one since we are interested in the shape of the pattern. The actual response magnitude of each device can be found by normalizing the response at normal incidence according to the data shown in Fig. 2.

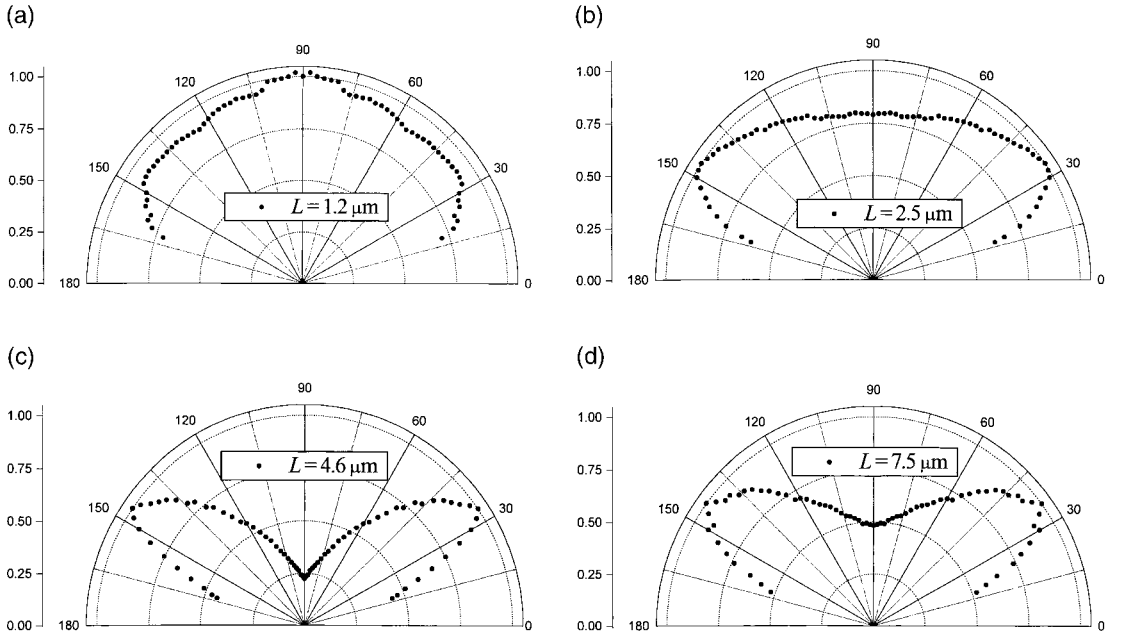

Fig. 4. Polarization-dependent signal ΔV as a function of the angle of incidence in the *E*-plane for devices with the antenna length *L*: (a) $L = 1.2$ μm, (b) $L = 2.5$ μm, (c) $L = 4.6$ μm and (d) $L = 7.5$ μm.

For the shortest antenna length that corresponds roughly to the $\lambda/2$ resonance ($L = 1.2$ μm, Fig. 4a) we observe only a major lobe with a maximum at normal incidence. This major lobe is broad, and starts to separate into two side-lobes as the length increases ($L = 2.5$ μm, Fig. 4b). The pattern for the length that corresponds to a "2λ" current distribution ($L = 4.6$ μm, Fig. 4c) shows clearly two side lobes with a sharp minimum for normal incidence. As the length is further increased, the center of the pattern increases again, suggesting the emergence of a broadened main lobe ($L = 7.5$ μm, Fig. 4d).

The results presented here show that infrared antennas possess receiving patterns that are strongly dependent on the geometry of the antenna. A qualitative agreement can be found with the expected single lobe for short antennas (for example $\lambda/2$) and a double-lobe structure for the 2λ antenna. Several characteristics of our devices and measurements are likely to explain the broad major lobes observed and the location of the side lobes at large angles. First, the slowing of the current-wave propagation by the surface reactance of the metal results in the modification of the pattern and a reduction of the main lobe [14]. The receiving pattern will be also changed by the presence of the substrate. Finally, a broadening of the pattern is caused by the convolution by an angular window introduced by the focusing of the beam.

Contrary to the antenna signal ΔV, the polarization-independent part of the signal $V_{\min}$ does not exhibits a dependence on the antenna length. For the four lengths investigated, we measured dependence of the signal $V_{\min}$ that closely follows a cosine of the angle of incidence, as represented in Fig. 5 for $L = 2.5$ μm. This cosine dependence approximates the decrease in projected area of the detector as it is tilted.

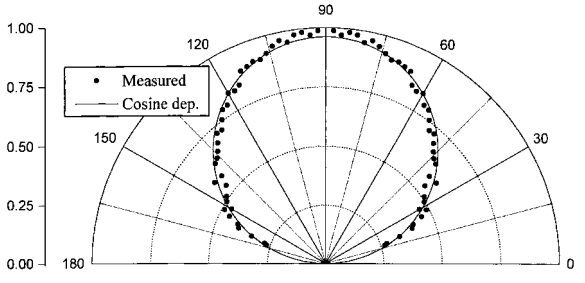

Fig. 5. Polarization-independent signal $V_{\min}$ as a function of the angle of incidence in the E-plane for an antenna length of $L = 2.5$ μm.

4.5. Measurements at 3.39 μm

Measurement of the signal ΔV as a function of the antenna length L was also performed at a wavelength of 3.39 μm (frequency of 88.5 THz), for antenna lengths L between 0.7 μm and 10 μm. The maximum signals were obtained for each device when the polarization was parallel to the antenna, and polarization ratios $V_{\max}/V_{\min}$ up to 5 were measured for devices with the shortest antenna, when illuminated through the substrate. The antenna signal ΔV as a function of L is plotted in Fig. 6. The shape of the curve closely resembles that measured at 10.6 μm (Fig. 2). The first resonance is suggested by the high response of the bolometer that has the shortest antenna. It is followed by a minimum for $L \approx 2.2$ μm, and by a second maximum with amplitude around 1/3 of the first maximum for $L \approx 3.5$ μm. This second maximum is again broadened on the side of longer

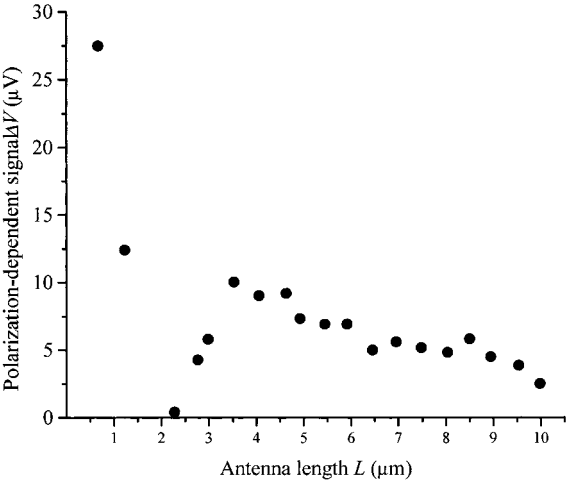

Fig. 6. Polarization-dependent signal ΔV as a function of the antenna length L at a wavelength of 3.39 μm. The curve is measured for illumination through the substrate at normal incidence.

antennas. Past this second resonance, the curve shows a slow decay without further notable oscillations.

In order to identify the resonances, we proceed at 3.39 μm as we did at 10.6 μm. The first minimum of the antenna response as a function of the length L is interpreted as the 2λ anti-resonance that exhibits a zero of the current distribution in the middle of the receiving antenna. This interpretation yields an apparent wavelength $\lambda_{app} \approx 1.1$ μm.

The scaling of the resonances between radiation at 10.6 μm and 3.39 μm gives rise to some questions. The ratio of the free-space wavelengths is 3.1 whereas the ratio of the apparent wavelengths is only around 2.3. Since Si has the same index of refraction to the third significant digit at the two wavelengths considered [20], it is unlikely that an effect in Si is the cause of the unexpected result. On the contrary, the thin isolating SiO_2 layer of our substrate possesses significantly different values of its index of refraction at the two wavelengths considered. The index of refraction n_{SiO_2} is around 1.4 at 3.39 μm and around 2.2 at 10.6 μm [20]. The influence of the SiO_2 layer on the effective index will consequently distort the expected scaling in the direction observed, i.e. a longer than expected resonant length at 3.39 μm because of a smaller effective index.

Consequently, we interpret the distorted scaling as the emergence of an effect that was neglected in the previous considerations at 10.6 μm. The 0.2-μm-thick SiO_2 layer on the top of our Si substrate influences the effective index of refraction n_{eff} that describes propagation on our antenna structure. The combination of two facts makes the effect more apparent at 3.39 μm than at 10.6 μm. First, the layer is thicker compared to the wavelength at higher frequencies (it has an optical thickness corresponding to more than 8% of the incident 3.39 μm free-space wavelength). Secondly, the index difference between Si and SiO_2 is larger at 3.39 μm than at 10.6 μm. Initial computer modeling of the structures confirms that a layer as thin as our SiO_2 layer influences the equivalent index of the substrate, and that the effect becomes more pronounced as the thickness of the layer increases.

In the following, we estimate the influence of the SiO_2 layer by taking into account the shortening of the wavelength by substrate reactance similarly as in Section 4.2. We first calculate the complex impedance of Au at 88.5 THz according to Eq. (1) based on the optical properties given in [15]. The ratio X_S/R_S increases with frequency and reaches 13.2 at 88 THz. The attenuation constant is then estimated according to Eq. (3) for a length $L_r = 6$ μm yielding $\alpha \approx 0.17$ μm^{-1}. Using Eqs. (2), (4) and the measured apparent wavelength $\lambda_{app} \approx 1.1$ μm, we estimate the effective wavelength to $\lambda_{eff} \approx 1.8$ μm. The equivalent index of refraction of the two-layer substrate is then estimated to be around $n_{eff} = \lambda_0/\lambda_{eff} \approx 1.9$. This value is situated between the indices of refraction of the two materials involved at the frequency considered ($n_{Si} = 3.43$, $n_{SiO_2} = 1.41$ at 88.5 THz). A more precise characterization of the equivalent index of refraction of our two-layer substrate will be the subject of future research.

4.6. Measurements in the visible

Antenna response at visible frequencies has been demonstrated in [21] with antenna-coupled MOM diodes. In order to investigate the high-frequency limit of operation of our antennas, we also investigated the response of our bolometers with different antenna lengths in the visible. For this purpose, we used the radiation of a HeNe laser at 632.8 nm. The lateral dimension of our antennas (200 nm), the minimum size of antenna (700 nm) and the increment in antenna length (about 500 nm) are clearly too high to obtain a resonance measurement as at longer wavelengths. However, the following observations indicate evidence of antenna operation at visible frequencies. For all the bolometers tested, with antenna lengths L between 0.7 and 6 μm, the highest responses are obtained for the polarization strictly parallel to the antenna. Polarization ratios V_{max}/V_{min} up to 3 are measured. When comparing these polarization ratios with the ones measured in the infrared (Table 1), one must keep in mind that in the visible the devices were illuminated from the air side, Si being opaque. In addition, the SiO_2 layer of the substrate has a much smaller absorption in the

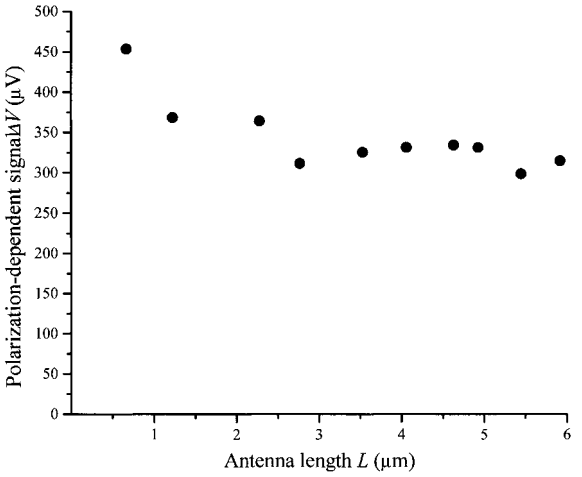

Fig. 7. Polarization-dependent signal ΔV of the bolometers as a function of the antenna length L at 632.8 nm. The points are measured for air-side illumination at normal incidence.

visible than in the infrared, resulting in a weaker unpolarized thermal response. The response of our antenna-coupled bolometers to visible light exhibits a higher polarization ratio than the response of the MOM diodes from [21], because the large low-frequency connections of our bolometers do not exhibit a preferred polarization direction. In the case of the MOM diodes, cross-polarized signals were enhanced by antenna responses from connections to the diode.

The only recognizable pattern of the response as a function of the antenna length in the visible is a slow decay as the length increases (Fig. 7). The highest antenna signal is measured for the shortest antenna. Its magnitude is about 1.5 times the signal measured for the longest antennas. A relatively slow decay past the two shortest antennas is observed. This suggests that the longer antennas act as infinite antennas and that an antenna response of the bolometer structure itself is superimposed on that of the Au structure. The length of the Nb structure is 800 nm, comparable with the wavelength of the visible incident radiation. Although we obtain significant polarization dependence in the visible, the results indicate that smaller structures are needed for an optimization of the response.

5. Conclusions

We have measured the response of dipole-antenna-coupled microbolometers as a function of antenna length at three different wavelengths: 10.6, 3.39 μm and 632.8 nm. Large antenna responses and polarization ratios were measured at each wavelength (Table 1).

Resonant lengths of receiving antennas have been determined at the two infrared wavelengths used in our study. The propagation constant has been determined by identifying the first minimum of the response as corresponding to a two-apparent-wavelengths long dipole. The effective wavelength for propagation of currents with THz frequencies on the antenna can be determined by an effective permittivity that is defined as for a transmission line. The value of the effective permittivity is located between the quasi-static approximation (average of the permittivity of air and of the substrate) and the high-frequency asymptotic value (permittivity of the substrate). The wavelength observed in the experiment is the effective wavelength further shortened by the significant high-frequency surface reactance of the metal. The complex surface impedance of the metal can be alternatively taken into account by the means of a complex conductivity of the metal.

The $\lambda/2$ resonance of the antenna thus occurs at a very short antenna length. The behavior of the curve for longer antennas suggests that the strong attenuation of antenna currents at infrared frequencies hinders the development of resonances for lengths past four to five effective wavelengths. Illumination through the substrate renders the most efficient coupling, and does not change the resonant lengths of the antennas.

Well-defined angular response patterns that can be related to the antenna length have been measured for 10.6 μm incident radiation. We measured a single broad lobe for the first resonant antenna length, and two side lobes for the first minimum. The antenna patterns are broadened and the side lobes are located at larger angles than would be expected for ideal dipoles in free space. This is probably caused by the influence of the large surface impedance of the metal and by the presence of the substrate.

Measurements of significant antenna-response in the visible demonstrate that antenna operation at even higher frequencies is possible. However, the observed trends suggest that the efficiency of the antennas decreases as the frequency increases (Table 1). Operation of antennas in the visible will require smaller structures with a similar aspect ratio.

Antenna-coupled detectors show promise as fast room-temperature polarization-sensitive sensors. Our measurements show a way toward the maximization of their responsivity by using proper resonant lengths in the design. They also uncover several aspects of the characteristics of the antennas, dependent on the illumination conditions, that need to be considered in the design of the sensors.

Acknowledgements

The authors acknowledge the support of the Ballistic Missile Defense Organization and Lockheed Martin Corporation.

References

[1] E.N. Grossman, J.E. Sauvageau, D.G. McDonald, Lithographic spiral antennas at short wavelengths, Appl. Phys. Lett. 59 (1991) 3225–3227.
[2] I. Codreanu, C. Fumeaux, D.F. Spencer, G.D. Boreman, Microstrip antenna-coupled infrared detector, Electron. Lett. 35 (1999) 2166–2167.
[3] N. Chong, H. Ahmed, Antenna-coupled polycrystalline silicon air-bridge thermal detector for mid-infrared radiation, Appl. Phys. Lett. 71 (1997) 1607–1609.
[4] I. Wilke, W. Herrmann, F.K. Kneubühl, Integrated nanostrip dipole antennas for coherent 30 THz infrared radiation, Appl. Phys. B 58 (1994) 87–95.
[5] C. Fumeaux, W. Herrmann, F.K. Kneubühl, H. Rothuizen, Nanometer thin-film Ni-NiO-Ni diodes for detection and mixing of 30 THz radiation, Infrared Phys. Technol. 39 (1998) 123–183.
[6] E.N. Grossman, L.R. Vale, D.A. Rudman, K.M. Evenson, L.R. Zink, 30 THz mixing experiments on high temperature superconducting Josephson junctions, IEEE Trans. Appl. Superconduct. 5 (1995) 3061–3064.
[7] T.H. Büttgenbach, R.E. Miller, M.J. Wengler, D.M. Watson, T.G. Phillips, A broad-band low-noise SIS receiver for submillimeter astronomy, IEEE Trans. Microwave Theory Tech. MTT 36 (1988) 1720–1725.
[8] H.P. Röser, H.W. Hübers, Schottky barrier devices for THz applications, in: J.M. Chamberlain, R.E. Miles (Eds.) New Directions in Terahertz Technology, NATO ASI series E 334, 119–125, Kluwer Academic Publishers, Boston, 1997.
[9] S.E. Schwarz, B.T. Ulrich, Antenna-coupled infrared detectors, J. Appl. Phys. 48 (1977) 1870–1873.
[10] Y. Yasuoka, T. Shimizu, K. Gamo, Fabrication of slot antenna coupled warm carrier detectors for millimeters wave radiation, Microelectron. Engng. 41/42 (1998) 445–448.
[11] G.D. Boreman, C. Fumeaux, W. Herrmann, F.K. Kneubühl, H. Rothuizen, Tunable polarization response of a planar asymmetric-spiral infrared antenna, Opt. Lett. 23 (1998) 1912–1914.
[12] R.W.P. King, H. Rowe Mimno, A.H. Wing, Transmission lines antennas and wave guides, Chapter 2, Section 29, Dover Publications, New York, 1965.
[13] M.Y. Frankel, S. Gupta, J.A. Valdmanis, G.A. Mourou, Terahertz attenuation and dispersion characteristics of coplanar transmission lines, IEEE Trans. Microwave Theory Tech. MTT 39 (1991) 910–915.
[14] D.B. Rutledge, S.E. Schwarz, A.T. Adams, Infrared and submillimeter antennas, Infrared Phys. 18 (1978) 713–729.
[15] M.A. Ordal, R.J. Bell, R.W. Alexander Jr., L.L. Long, M.R. Querry, Optical properties of Au, Ni, and Pb at submillimeter wavelengths, Appl. Opt. 26 (1987) 744–752.
[16] R.J. Bell, M.A. Ordal, R.W. Alexander Jr., Equations linking different sets of optical properties for nonmagnetic materials, Appl. Opt. 24 (1985) 3680–3682.
[17] M.I. Ali, K. Ehata, M. Kusunoki, S. Ohshima, Effect of surface impedance on the antenna properties in superconducting microstrip antenna, Physica C 325 (1999) 143–152.
[18] D.B. Rutledge, M.S. Muha, Imaging antenna arrays, IEEE Trans. Antennas Propagation AP 30 (1982) 535–540.
[19] J. Alda, C. Fumeaux, M.A. Gritz, D. Spencer, G.D. Boreman, Responsivity of infrared antenna-coupled microbolometers for air-side and substrate-side illumination, Infrared Phys. Technol. 41 (2000) 1–9.
[20] E.D Palik (Ed.), Handbook of optical constants of solids, Academic Press, New York, 1985, pp. 547ff, 749ff.
[21] C. Fumeaux, J. Alda, G.D. Boreman, Lithographic antennas at visible frequencies, Opt. Lett. 24 (1999) 1629–1631.